Nonlinear Damage Accumulation Rule for Solder Life Prediction Under Combined Temperature Profile With Varying Amplitude

Ying Chen, *Member, IEEE*, Weiyang Men, Zenghui Yuan, Rui Kang, *Member, IEEE*, and Ali Mosleh, *Member, IEEE*

Abstract—Due to a mismatch of the coefficient of thermal expansion, electronic solder joints experience cyclic shear strain, which ultimately leads to fatigue failure. Traditional predictions of solder joint thermal fatigue life that use the experimental data or the physics-of-failure model often assume a regular profile. For complex temperature profiles, the linear accumulation rule is typically used to integrate the superposition effect. However, the linear rule was proved not applicable to most of the complex loading or temperature conditions. Based on the damage curve theory and the fatigue crack propagation theory, a novel nonlinear accumulation rule has been deduced for solder joint life predictions under irregular profiles, which were composed of two standard temperature cycles and may be experienced by phased-mission system. Four groups of experiments were conducted for ball grid array package solder joints with different dimensions and materials to determine parameters of the proposed nonlinear accumulation rule. The finite-element simulation method was used to extend this rule to more general cases for application. Compared to Miner's linear accumulation rule, prediction of solder joint thermal fatigue life via the proposed nonlinear accumulation rule is closer to the accelerated life test results of real-world electronic solder joints under a combined temperature profile.

Index Terms—Combined temperature profile, nonlinear damage accumulation rule, solder joint, thermal fatigue life.

NOMENCLATURE

CTE	Coefficient of thermal expansion.
PoF	Physics-of-failure.
PMS	Phased-mission system.
PBGA	Plastic ball grid array.
CCGA	Ceramic column grid array.
DCA	Damage curve analysis.
DLDR	Double linear damage rule.
IDSA	Incremental damage superposition approach.
PCB	Printed circuit board.
BGA	Ball grid array.
FEA	Finite-element analysis.
N	Number of cycles to failure.
σ	Stress of temperature.
D	Fatigue damage.
l	Crack length.
m	Number of damage nuclei.
r	Damage factor.
D_S	Diameter of the solder joint.
L_D	Ratio of crack expansion length.
a	Constant.
b	Constant.
N_f	Fatigue life.
γ	Material characteristic strength coefficient.
E	Young's modulus.
σ_f	Fatigue strength factor.

I. INTRODUCTION

SOLDER joints serve as electrical connections, as mechanical support, and to aid heat dissipation of electronic packages. During operation, solder joints are typically subjected to cyclic loading due to a mismatch of thermal expansion coefficients between component and the board onto which the component is mounted. Creep, fatigue, and their interactions are considered to be the main mechanisms leading to the eventual thermal fatigue failure of solder joints. The experimental data and thermal fatigue life PoF models can both be used to predict the life of solder joints under regular or standard temperature cycle. In reality, however, electronic devices often work under irregular or complex temperature profiles with varying amplitudes. For example, one of the real-world cases for electronic devices that work in a PMS is aircraft flight, which involves taxi, takeoff, ascent, level-flight, descent, and landing phases [1]. During each phase, the system has to accomplish a specified task and may be subjected to different temperatures and vibration environments. Thus, the

temperature profile of this type of system is irregular compared to a standard temperature cycle. Complex temperature profiles increased the challenges for both model and prediction of solder joint reliability.

The problem of solder joint reliability is complicated due to electronic devices suffering various types of loads or environments, such as thermal, vibrational, and electrical power. In addition, the profile of each load is not always regular. Many studies have been conducted to predict different stresses applied on solder joints, either simultaneously or sequentially. The damage accumulation method has usually been used to calculate the final effect of combined environments or loads [2], [3]. Many types of accumulation rules exist, such as linear, bilinear, and nonlinear. Among them, Miner's linear rule is the most popular in both research and engineering [4]. Barker et al. [5] used Miner's rule to superpose vibration and thermal fatigue damage caused by both inelastic and elastic strains of electronic solder joints. Yang et al. [6] studied the life-prediction approach of solder joints via the finite-element method under combined loading of thermal and vibration. Based on the linear damage superposition approach at high temperature, the total damage was divided into two parts, which were time-independent damage (fatigue damage), and time-dependent damage (creep damage). Pang et al. [7] studied the fatigue failure of PBGA package solder joints under vibration loading at different accelerations, using Miner's rule for cumulative fatigue damage and vibration fatigue failure life. Perkins and Sitaraman [8] used Miner's rule to predict the fatigue failure of CCGA package solder joints under Sinusoidal vibration with sweeping frequency.

For the problem of predicting the reliability of solder joints under a complex temperature profile, the conventional method is to segment that into single or regular profiles and then integrate their damage effects. Using the numerical method, Pei et al. [9] analyzed the solder creep energy under a complex temperature cycle during which mini-cycles occurred at the upper dwell. They decomposed the two simple temperature cycles from the complex cycle and studied their creep energy. Chai et al. [10] listed different profile segmenting schemes to predict the solder fatigue life under field thermal conditions, which were complex temperature cycles composed of three temperature dwell points each. Miner's rule was used to superpose the damage of the segmented cycles. The life prediction results of the preferred segmenting scheme were closest to their physical test results. However, if the profile changed, a new cycle segmentation method had to be studied.

Recently, more studies found that the linear accumulation rule was not applicable to most complex loading conditions. Basaran and Chandaroy [11] studied a combined loading situation by superposing the damage due to vibration and thermal loads using Miner's rule. The results showed that Miner's rule significantly underestimated the total damage, and consequently, overestimated the fatigue life, therefore, strongly suggesting that Miner's rule cannot be used for calculating combined environment damage values. Perkins and Sitaraman [12] summarized the problems of Miner's rule, which included insensitivity to the sequence of load steps and nonconservatism. The authors investigated

the sequence loading effects, which included vibration and temperature in sequence and found that the Miner's cumulative linear damage rule was incapable to account for the sequence effect. Yang et al. [13] focused on the life of Sn–Ag–Cu (SAC) solder joints in isothermal mechanical cycling with varying amplitudes. Solder joints were cycled at one of the loads for a specific number of cycles and then cycled at another amplitude until failure. Results showed that Miner's rule of linear damage accumulation tended to overestimate the room-temperature fatigue life of SAC solder joints in mild–harsh loading sequences, while underestimating their life in mild–harsh sequences. Research by Borgesen et al. [14] showed strong deviations from the linear damage accumulation for sequences of a single type of loading with different amplitudes.

Since the linear accumulation rule was not applicable, some studies have used alternate damage accumulation models. Perkins and Sitaraman [12] developed a nonlinear damage accumulation model to account for sequence effects of thermal fatigue and vibration fatigue. Lin and Teng [15] used the Miner's linear rule to study the sequence effect of high–low and low–high stresses on the creep fatigue life of SAC solder. Creep tests were conducted under two-step loading, using various combinations of stress and temperature, and a nonlinear cumulative creep damage model was proposed. Jin et al. [16] used the DCA and DLDR to account for the constant stress amplitude and three different two-level block-loading conditions. Various studies found other strategies to superpose different loads instead of using accumulation rules. Qi et al. [17] presented an IDSA to predict solder joint life under combined thermal cycling and vibration loading conditions, by taking temperature effects and loading interactions into account. Test results showed that PBGA solder joint would fail far earlier under combined loading than with either separate temperature cycling or room temperature vibration loading. Traditional linear superposition was reported to overpredict the solder joint fatigue life since it neglected the interaction effects of two different loads. Basaran and Chandaroy [11] proposed a constitutive model based on unified damage mechanics for the assessment of solder joint fatigue under simultaneous thermal and vibration loading. Manson and Halford [18] and Singh [19] had also used crack initiation and crack propagation as damage parameters to account for sequence effects and other abnormalities.

Most of the nonlinear accumulation rules proposed in the previous studies were applied for conditions under combined thermal and vibration loading. Only few researchers contributed to the nonlinear accumulation rule under combined temperature profile with different thermal stresses, which is a common condition in PMS. Marco and Starkey [20] presented a damage curve theory, which inferred that the relationship between the damage and failure cycle is exponential; however, this paper was limited to qualitative analysis. Kommers [21] and Huang [22] proposed nonlinear fatigue damage accumulation models based on the material performance degradation theory, which had good physical bases, but the interaction and sequential effects of multistage loads had not been taken into account. Halford [23] and Niu et al. [24] studied the issues about cycle lag, cycle creep, and cycle

softening that occurred in combined temperature profile. The authors presented some accumulation rules based on energy theory, which were more realistic, however, the formulas were very complicated and the parameters were often difficult to determine.

Currently, the most common method used to study damage accumulation under a combined temperature profile still remains Miner's rule, due to the impracticality of the nonlinear rules proposed before. New strategies need to be developed. In this paper, a nonlinear accumulation rule has been developed for solder joint life prediction under combined profile, which is composed of two standard temperature cycles, based on both damage curve theory and fatigue crack propagation theory. Experimental and simulation methods were adopted to determine the parameters of the proposed nonlinear accumulation rule and to extend it for more general conditions. The new accumulation rule considered both superposed and sequential effects and the resulting form is even simpler.

The remainder of this paper is organized as follows. Section II presents the nonlinear accumulation rule from a fatigue crack and propagation point of view. Section III discusses the experimental procedures and results of data analysis to form the complete accumulation rule. Section IV introduces the FEA simulation-based method of solder joint thermal fatigue prediction and investigates the relationship of solder joint dimension and material with the proposed nonlinear accumulation rule. A real-world case is also presented to compare the accumulation results with accelerated test results. Section V provides the conclusion as well as directions for future work.

II. NONLINEAR ACCUMULATION RULE

A. General Form

The linear accumulation rule, which is also called Miner's rule, can be provided as

$$\frac{1}{N} = \frac{1}{N_1} + \frac{1}{N_2} \tag{1}$$

where σ represents the stress that leads to fatigue failure. N_1 represents the number of cycles to failure under σ_1, N_2 represents the number of cycles to failure under σ_2, and N represents the number of cycles to failure under combined stress; note that the σ_1 and σ_2 are in sequence, which is shown in Fig. 1(a).

It has been studied that the failure of solder joint under temperature change is due to thermal fatigue. The more temperature cycles the joint performs, the more stress level will be exerted on the solder joint, resulting in higher damage velocity. Fig. 1(b) shows the combined temperature profile, corresponding to the combined load profile in Fig. 1(a). A standard temperature profile contains two temperature values and corresponds to one fatigue stress.

For the stresses σ_1 and σ_2, fatigue damage can be calculated via [25]

$$D = m_1 r_1 N_1^{a_1} = m_2 r_2 N_2^{a_2} \tag{2}$$

where D represents the fatigue damage, m_1 and m_2 represent the number of damage nuclei under σ_1 and σ_2, r_1 and r_2
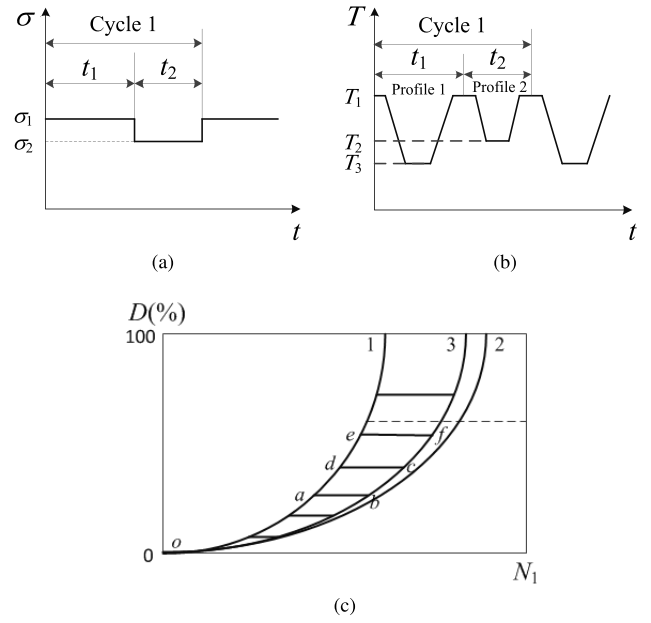

Fig. 1. Loading profile and damage curve of combined conditions. (a) Combined load profile. (b) Combined temperature profile. (c) Damage curve.

represent the damage factors, which differ according to stress level, and a_1 and a_2 are constants to be determined.

If profiles 1 and 2 changed alternately, the new temperature profile would be a combination of one profile 1 and one profile 2 for one cycle, and the fatigue stress would be a combination of t_1 time of σ_1 and t_2 time of σ_2, which is a new loading period; the combined loading profile, combined temperature profile, and damage curve are depicted in Fig. 1.

Here, curves 1 and 2 show the fatigue damage curve under σ_1 and σ_2, respectively, and their fatigue damages are

$$D_1 = m_1 r_1 N_1^{a_1}, \quad D_2 = m_2 r_2 N_2^{a_2}. \tag{3}$$

For the same material, $a_1 = a_2 = a$. When σ_1 is applied first, the number of damage nuclei (m_1) is produced and the damage curve begins from o to a; in other words, curve oa represents the damage path. As the stress changes to σ_2 at point a, the damage curve is not curve 2, but curve 3, and the damage is $D_3 = m_1 r_2 N_2^a$. Curve bc represents the damage path under stress σ_2. As stress changes back from σ_2 to σ_1, the damage curve will be de. Furthermore, the damage equivalent value of bc under σ_2 is equal to the damage equivalent value of ad under σ_1.

Furthermore, every cycle of the combined temperature profile contains one profile 1 cycle and one profile 2 cycle. This indicates that the number of cycles to failure under σ_1 was equal to the number of cycles to failure under σ_2 in the combined temperature profile, which equals N, then

$$m_1 r_1 N_1^a = m_1 r_1 N^a + m_1 r_2 N^a \tag{4}$$

where $m_1 r_1 N_1^a$ represents the damage value under σ_1, like curve oe, and $m_1 r_1 N^a + m_1 r_2 N^a$ represents the damage value under combined stress σ, like $oa + bc + de$. As discussed above, these two damage values are equal. Then, r is proportional to

the stress σ; therefore, (4) can be replaced by

$$N = \frac{N_1}{(1 + r_2/r_1)^{\frac{1}{a}}} = \frac{N_1}{(1 + \sigma_2/\sigma_1)^{\frac{1}{a}}}. \qquad (5)$$

When fatigue happens to the solder joint under stress σ, and $\sigma = \gamma (N)^b$, where γ represents the material characteristic strength coefficient, b is a constant to be determined, and N represents characteristic cycles to fatigue. For the same solder joint material, $\gamma_1 = \gamma_2$, $b_1 = b_2$, then

$$\frac{\sigma_1}{\sigma_2} = \left(\frac{N_1}{N_2}\right)^b. \qquad (6)$$

Then

$$N = \frac{N_1}{(1 + (N_2/N_1)^b)^{\frac{1}{a}}}. \qquad (7)$$

Equation (7) is the general form of the accumulation rule for a combined profile with two temperature cycles. Here, b and a are constants to be defined by the following part with either experimental or simulation data. N_1 and N_2 are the numbers of cycles to failure under stress levels of the two standard temperature profiles, respectively, which can be obtained via experiment data, simulation data, or the PoF model.

B. Parameter Calculation

The crack development model of solder joint can be given by [26] and [27]

$$l = l_0 + (0.7D_S - l_0)\left(\frac{N_l}{N_f}\right)^{\frac{2}{3}N_f^{0.4}} \qquad (8)$$

where l represents the crack length of solder joint, l_0 represents the initial crack length, D_S represents the diameter of solder joint, N_f represents the cycle numbers to fatigue failure, and N_l represents the cycle numbers when the crack length reaches l. When the solder joint falls off, the crack length is equal to the diameter of the solder joint, which denotes failure in principle. However, in order to leave a security margin, the solder joint is considered to have failed when the crack length reaches 70% of the diameter of the solder joint, $l_f = 0.7D_S$, based on GB/T6398 [28]. Then, the crack expansion factor L_D is defined as the ratio between the crack expansion length and the crack length at the time when failure happens, which is

$$L_D = \frac{l_0 + (0.7D_S - l_0)\left(\frac{N_l}{N_f}\right)^{\frac{2}{3}N_f^{0.4}}}{0.7D_S}. \qquad (9)$$

Since the initial crack length is small compared to the expansion crack length, we assumed that $l_0 = 0$; at the crack expansion phase, the crack expansion ratio was equal to the damage value D [29], where $D = mrN_l^a$, then

$$\left(\frac{N_l}{N_f}\right)^{\frac{2}{3}N_f^{0.4}} = mrN_l^a. \qquad (10)$$

If N_1 and N_2 could be achieved by two temperature cycle experiments, then if the cycles were n_1 and n_2, respectively, the damage values would be

$$D_1 = \left(\frac{n_1}{N_1}\right)^{\frac{2}{3}N_1^{0.4}} = m_1 r_1 n_1^a, \quad D_2 = \left(\frac{n_2}{N_2}\right)^{\frac{2}{3}N_2^{0.4}} = m_2 r_2 n_2^a \qquad (11)$$

where $m_1 = m_2$, and

$$\frac{D_1}{D_2} = \frac{r_1 n_1^a}{r_2 n_2^a} = \frac{\left(\frac{n_1}{N_1}\right)^{\frac{2}{3}N_1^{0.4}}}{\left(\frac{n_2}{N_2}\right)^{\frac{2}{3}N_2^{0.4}}}. \qquad (12)$$

When $(D_1/D_2) = 1$, in other words, when both resulting damage values were equal, $(r_1/r_2) = (\sigma_1/\sigma_2) = ((N_1/N_2))^b$, then

$$\left(\frac{N_1}{N_2}\right)^b \left(\frac{n_1}{n_2}\right)^a = \frac{\left(\frac{n_1}{N_1}\right)^{\frac{2}{3}N_1^{0.4}}}{\left(\frac{n_2}{N_2}\right)^{\frac{2}{3}N_2^{0.4}}}. \qquad (13)$$

Log on both side of (13), then

$$b \ln \frac{N_1}{N_2} + a \ln \frac{n_1}{n_2} = \frac{2}{3}N_1^{0.4} \ln \frac{n_1}{N_1} - \frac{2}{3}N_2^{0.4} \ln \frac{n_2}{N_2} \qquad (14)$$

$$b \ln \frac{N_1}{N_2} + a \ln n_1 - a \ln n_2 = \frac{2}{3}N_1^{0.4} \ln n_1 - \frac{2}{3}N_1^{0.4} \ln N_1$$
$$- \frac{2}{3}N_2^{0.4} \ln n_2 + \frac{2}{3}N_2^{0.4} \ln N_2 \qquad (15)$$

$$\ln n_1 \left(a - \frac{2}{3}N_1^{0.4}\right) = \ln n_2 \left(a - \frac{2}{3}N_2^{0.4}\right)$$
$$- \left(b \ln \frac{N_1}{N_2} + \frac{2}{3}N_1^{0.4} \ln N_1\right.$$
$$\left. - \frac{2}{3}N_2^{0.4} \ln N_2\right). \qquad (16)$$

N_1, N_2, n_1, and n_2 can be obtained via experiment or simulation; then, the coefficients a and b can be fitted, and the nonlinear accumulation rule of (7) is determined.

III. EXPERIMENTS

This section mainly shows the experimental procedures for obtaining N_1, N_2, n_1, and n_2, as well as the conducted data fitting for calculating coefficients a and b according to a real-life case. The results show that the proposed nonlinear accumulation rule enables a closer prediction of solder joint life to the real situation than Miner's rule.

A. Temperature Profile

The temperature profile used in this paper is used in a PMS, where a helicopter is involved in parking, taxi, takeoff, ascent, level-flight, descent, and landing phases. FIDES guide 2009 [30] contains a detailed description on how to construct a life profile to be used for reliability prediction of electronic systems. A navigation computer onboard a VIP helicopter, which was mounted on the cockpit, was chosen as an example
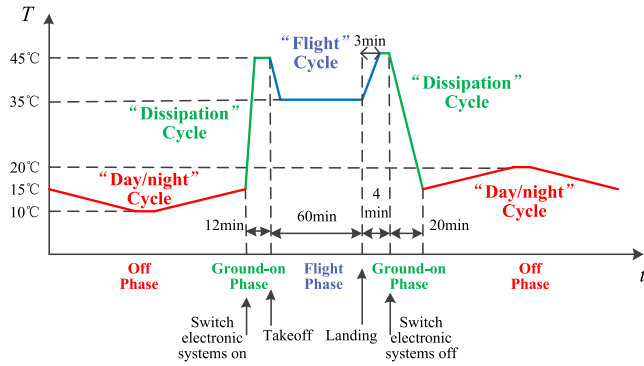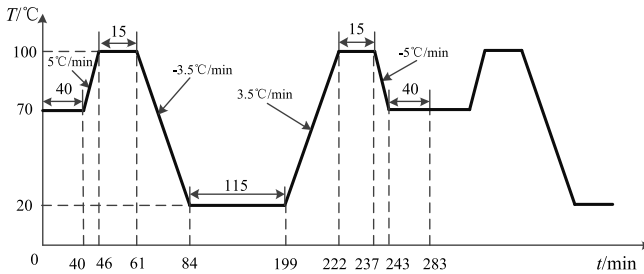
Fig. 2.   Temperature profile in FIDES.

Fig. 3.   Combined temperature profile (profile 1).

to build phases in the life profile beginning at the life sequence of the profile. There are three cycles in the life profile of this example. The "flight" cycle ranges from 45 °C to 35 °C, the "dissipation" cycle ranges from 15 °C to 45 °C, and also the "day/night" cycle ranges from 20 °C to 10 °C. These are shown in Fig. 2.

Another example is a data collection and measuring system that was installed near the engine, and that also uses different phases of a task; the resulting life temperature profile (profile 1) is shown in Fig. 3. There are two cycles in Fig. 3: the "flight" cycle ranges from 100 °C to 20 °C and the "dissipation" cycle ranges from 70 °C to 100 °C. The "day/night" cycle has been omitted in this case due to its small impact on system life. During hot day, the ground temperature can reach 55 °C, and since the electronic device was installed inside, considering a temperature difference of 15 °C, this would be 70 °C. When the engine starts to work, the temperature increases to 100 °C. During the flight phase, it will drop to 20 °C due to a combination of various factors that influence temperature, which include environmental temperature at an altitude of 1000 m, the engine, and the ram-air cooling system.

The detailed values of profile 1 are shown in Table I. The lower dwell was at 20 °C for 115 min, while the medium dwell was at 70 °C for 80 min. There were two upper dwells at 100 °C for 15 min each time. The overall cycle duration was 283 min, and the rates of temperature change were 3.5 and 5 °C/min.

The complex temperature profile can be divided into two standard temperature cycles (profiles 2 and 3), which are shown in Fig. 4, and their detailed values are shown in Table II. The lower dwell of the temperature profile 2 was 20 °C for 115 min, and the upper dwell was 100 °C for 15 min.

TABLE I
DETAILED VALUES OF TEMPERATURE PROFILE 1

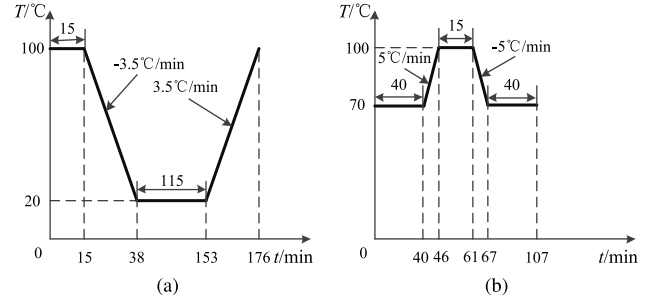|	Temperature (°C)	Duration time (min)
1	70	40
2	Ascending	6
3	100	15
4	Descending	23
5	20	115
6	Ascending	23
7	100	15
8	Descending	6
9	70	40

Fig. 4.   Two standard temperature profiles. (a) Temperature profile 2. (b) Temperature profile 3.

TABLE II
DETAILED VALUES OF TWO STANDARD TEMPERATURE PROFILES

N	Standard temperature profile 2		Standard temperature profile 3	
	Temperature (°C)	Duration time (min)	Temperature (°C)	Duration time (min)
1	100	15	70	80
2	Decreasing	23	Increasing	6
3	20	115	100	15
4	Increasing	23	Decreasing	6
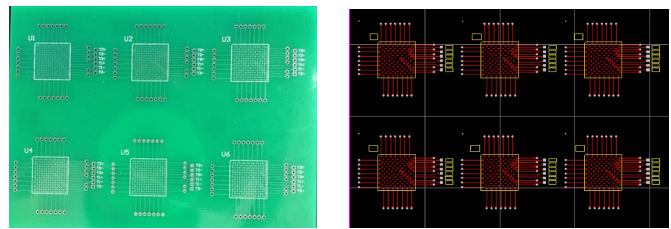
Fig. 5.   Test specimen.

The overall cycle duration was 176 min, and the rate of temperature change was 3.5 °C/min. For temperature profile 3, the lower dwell was 70 °C for 80 min, and the upper dwell was 100 °C for 15 min. The overall cycle duration was 107 min, and the rate of temperature change was 5 °C/min.

B. Test Specimen

To obtain the coefficients needed for (7), experiments were conducted and test specimens were produced. Chips were surface-mounted on PCBs with 96.5Sn3.5Ag and 96.5Sn$_3$Ag0.5Cu solder. Each test board had six BGA package chips (U1–U6), which is shown in Fig. 5. The dimension of
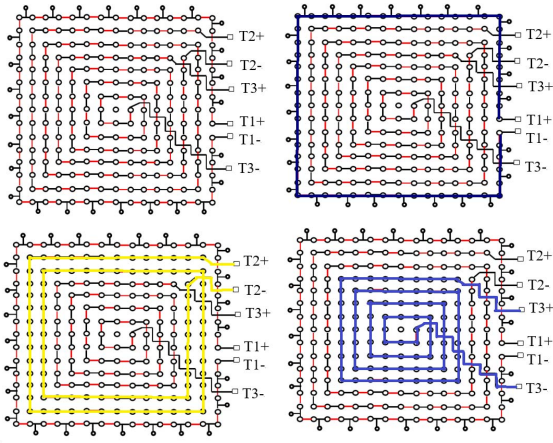
Fig. 6. Three daisy chains.

Fig. 7. Temperature chamber and test board within the chamber.

Fig. 8. Resistance of the T1 daisy chain in 12 chip samples under profile 1 of group 1.

these BGA chips was 16 mm × 16 mm. The FR4 laminate test boards had a thickness of 2.3 mm, and exposed copper surfaces were coated with organic solderability preservative finish. Each experimental group had two boards (A1 and A2). The BGA chips were mounted on the test board and an electrical resistance network that could be monitored for failure when the temperature cycling condition had been created.

The solder joint network created three daisy chains, which are shown in Fig. 6, named, T1, T2, and T3. The resistance of the daisy chain was equal to the sum of the resistances of all solder joints contained within. The solder joints of different daisy chains were under different thermal expansion mismatch conditions. Among them, the daisy chain under the most severe condition would be the first one to fail and its resistances were representations of the solder joints' thermal fatigue lives. The diameters of solder joint were 0.25 and 0.5 mm. Four groups of experiments were conducted: 1) group 1, 96.5Sn3.5Ag solder joint with diameter of 0.5 mm; 2) group 2, 96.5Sn3Ag0.5Cu solder joint with diameter of 0.5 mm; 3) group 3, 96.5Sn3.5Ag solder joint with diameter of 0.25 mm; and 4) group 4, 96.5Sn3Ag0.5Cu solder joint with diameter of 0.25 mm.

C. Device Setup and Experiment Description

The combined temperature cycling profile was achieved with a temperature chamber, and no spatial thermal gradient was assumed through the device. The chamber and the test boards are shown in Fig. 7.
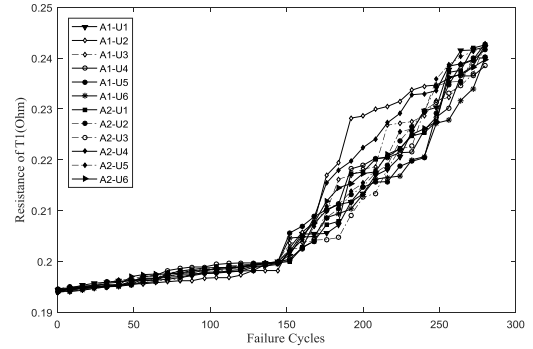
The resistance values of daisy chains T1, T2, and T3 were measured with a resistance tester to determine the time when failure occurred, which was then sent to the computer for analysis. If the resistances of the first failed daisy chain of the chip in three temperature experiments were identical, they would have the same fatigue damage D; their cycles were recorded as n (profile 1), n_1 (profile 2), and n_2 (profile 3), respectively. Interconnecting failure was defined as a 20% increase in nominal resistance of these three daisy chains, which means that at least one of the solder joints had failed ($l_f = 0.7D_S$), based on GB/T6398 [28]. For the first daisy chain to failure, when the three profiles have the same resistance, the cycle numbers when the value first reached a 20% increment under each profile was recorded. This resulted in the failure cycle N (profile 1), N_1 (profile 2), and N_2 (profile 3), respectively.

D. Results and Discussion

With every experimental group, there were two test boards that had six chips mounted each. Within the same group, 12 resistance values of each type of daisy chain existed. The resistances of these 12 T1 daisy chains for the combined temperature profile (profile 1) of group 1 are shown in Fig. 8.

Fig. 8, furthermore, shows that the same resistance value of the T1 daisy chain reached 20% increase (0.2394 Ω at Table III) at about 280 cycles under profile 1 in group 1. At about 150 cycles, there was an inflection point. The resistance increased gradually before this point and the plastic strain occurred due to the difference in CTE between different material layers; however, no fatigue damage came into being at this stage. After that point, the plastic strain accumulation exceeded the threshold and fatigue damage occurred at the stress concentration zone of the solder joint; the resistance of T1 had a higher increasing speed and the data were more dispersed at this stage. Generally, these 12 groups of data had good uniformity. The medium value of these 12 groups of data was used to analyze the accumulation rules.

Fig. 9 shows the resistance change of daisy chains T1, T2, and T3 in experimental group 1 under the three temperature profiles.

Fig. 9 shows that under temperature profile 1, the resistance had the highest increasing speed, and the value was lowest

n (cycles)	n_1 (cycles)	n_2 (cycles)	Resistance (Ohm)
0	0	0	0.1942
8	12	88	0.1946
16	24	100	0.1948
24	36	120	0.1950
30	48	128	0.1952
38	60	142	0.1955
50	84	202	0.1963
64	108	244	0.1969
80	120	308	0.1976
110	156	372	0.1985
120	180	408	0.1990
144	206	466	0.2000
152	210	488	0.2028
160	216	498	0.2031
176	228	576	0.2098
208	270	712	0.2197
216	278	744	0.2211
240	312	840	0.2298
282	336	912	0.2394

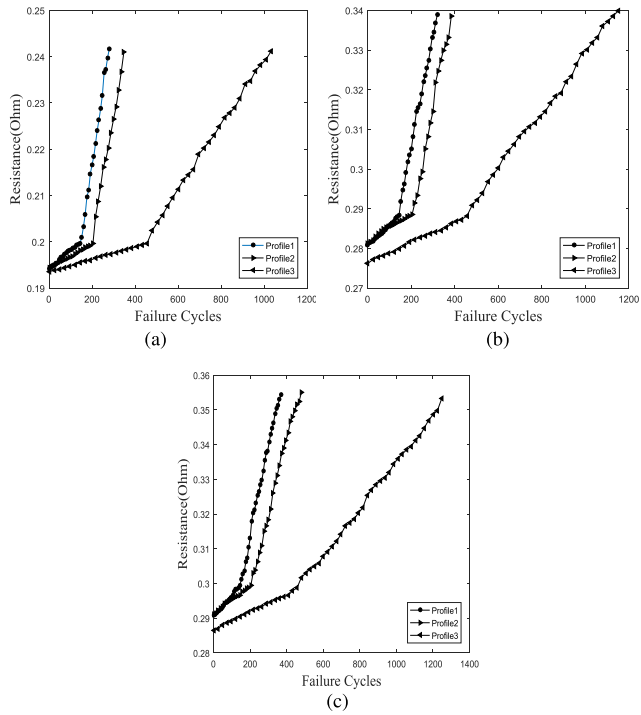Fig. 9. Resistance changes of daisy chains T1, T2, and T3 in experimental group 1 under three temperature profiles. (a) T1. (b) T2. (c) T3.

Fig. 10. Resistance changes of daisy chain T1 of the four groups of experiments under (a) profile 1, (b) profile 2, and (c) profile 3.
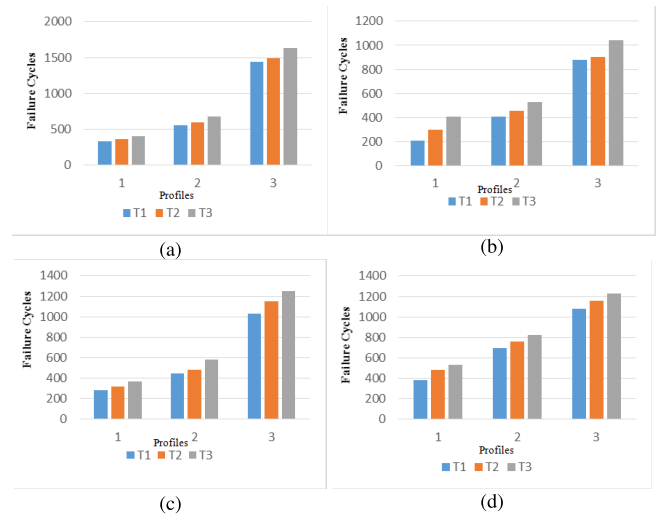
Fig. 11. Histogram of the failure cycles of daisy chains T1, T2, and T3. (a) Group 1. (b) Group 2. (c) Group 3. (d) Group 4.

under temperature profile 3. The results verified the argument mentioned above (4) in Section II-A, where every cycle of the combined temperature profile (profile 1) contained one profile 2 cycle and one profile 3 cycle; therefore, the failure cycle under profile 1 should be smaller than the other two. Furthermore, the failure speed under profile 3 was the lowest due to its smaller temperature difference compared to profile 2.

Fig. 10 shows the resistances of daisy chain T1 of the four experimental groups under profiles 1, 2, and 3, respectively.

Fig. 10 shows that the failure speeds of the same daisy chain under the same profile differed in different groups.

This indicates that the parameters *a* and *b* in (7) are related to the material and dimension of the solder joint. This relationship will be deeply investigated in Section IV-C.

Fig. 11 shows a histogram of the failure cycles of daisy chains T1, T2, and T3 under three profiles in the four groups of the experiment.

The cycle numbers in Fig. 11 show values when the daisy chains completely failed, which means that the daisy chains were open and the resistances were infinite. The results showed that the daisy chain T1 was the first one to fail under each profile in each group. The reason is that daisy chain

TABLE IV
VALUES OF A AND B AND GOODNESS OF FIT

Parameter	Value
a	2.759
b	-0.867
SSE	0.0028085
R-square	0.9581
Adjusted R-square	0.9557
RMSE	0.05586

T1 was installed on the outermost side of the chip of Fig. 6, which has maximal strain under the same thermal stress. As mentioned in Section III-B, daisy chain T1 was under the most severe thermal expansion mismatch conditions, and its resistances represented the thermal fatigue lives of solder joints of the chips. The resistances and failure cycles of daisy chain T1 under three profiles in four groups have been recorded for data fitting purposes.

E. Data Fitting

The experimental data were verified and n, n_1, and n_2 were picked up at the time when the resistances of daisy chain T1 in three experiments with profiles 1, 2, and 3 were identical. For example, for experiment group 1, the data are shown in Table III.

Table III shows that when the resistance T1 reached a 20% increase for the first time, n_1 and n_2 were 336 and 912, respectively, which represents the fatigue failure cycles N_1 and N_2 in (16). Furthermore, the failure cycle under combined profile was 282, which was the real value that was used for comparison with the calculated value.

Data fitting has been processed with MATLAB, and a and b in (16) are shown in Table IV.

Here, SSE represents the sum of squares due to error, while R-square represents the coefficient of determination. Adjusted R-square represents the degree-of-freedom adjusted coefficient of determination, and RMSE represents the root-mean-squared error.

Then, the nonlinear accumulation rule for the complex temperature profile for group 1 (which is 96.5Sn3.5Ag solder joint with a diameter of 0.5 mm) could be integrated as

$$N = \frac{N_1}{(1 + (N_2/N_1)^{-0.867})^{\frac{1}{2.759}}}. \tag{17}$$

All of the other three accumulation rules for the other three groups could be fitted with the same method

$$N = \frac{N_1}{(1 + (N_2/N_1)^{-1.122})^{\frac{1}{2.809}}} \quad \text{(Group2)} \tag{18}$$

$$N = \frac{N_1}{(1 + (N_2/N_1)^{-0.841})^{\frac{1}{2.857}}} \quad \text{(Group3)} \tag{19}$$

$$N = \frac{N_1}{(1 + (N_2/N_1)^{-1.137})^{\frac{1}{2.763}}} \quad \text{(Group4)}. \tag{20}$$

F. Discussion

Table V shows the failure cycles and damage ratios of daisy chain T1 under three profiles in four groups of this experiment.

TABLE V
FAILURE CYCLES AND DAMAGE RATIOS OF DAISY CHAIN T1

Group	Profile	Failure cycles of T1	Damage ratios	Damage sum under profile 2 and 3
1	1	282	1	
	2	336	0.84	1.15
	3	912	0.31	
2	1	184	1	
	2	216	0.85	1.18
	3	554	0.33	
3	1	232	1	
	2	270	0.86	1.21
	3	654	0.35	
4	1	338	1	
	2	412	0.82	1.25
	3	780	0.43	

TABLE VI
FAILURE CYCLES FROM EXPERIMENT AND TWO ACCUMULATION RULES

Group	Experiment cycles	Miner's rule cycles	Error ratios	Proposed nonlinear rule cycles	Error ratios
1	282	246	-12.8%	296	5.0%
2	184	155	-15.8%	194	5.4%
3	232	191	-17.7%	236	1.7%
4	338	270	-20.1%	357	5.6%

This damage ratio indicates the level of damage that occurred in daisy chain T1 under profiles 2 and 3 compared to profile 1 when daisy chain T1 failed under profile 1.

According to Miner's rule, the sum of the damage under profiles 2 and 3 should be equal to the damage under profile 1. However, Table V shows that those two values were not equal, the damage sum was larger, and the maximal error ratio reached 25% in this experiment, indicating that the linear accumulation rule was not applicable for this case.

Table VI shows the failure cycles that were obtained from this experiment, which are failure cycles of T1 under profile 1, and calculated by Miner's rule and the proposed nonlinear rule of the four groups. The error ratios are also listed in Table VI.

Table VI shows that the failure cycles calculated with Miner's rule were 20% below the experiment values at most. However, the error between the failure cycles calculated by the proposed nonlinear rule and experimental values could be controlled within 6%. The prediction of solder joint life with the proposed nonlinear accumulation rule was closer to the actual situation.

IV. FEA SIMULATION

The experimental results were most realistic; however, both time and cost of the experiment were quite significant for aviation products due to the large failure cycle numbers. Therefore, simulation is still the main technology applied for engineering. This section is mainly to show the simulation method for solder joint thermal fatigue, and to explore the relationship between parameters a and b with the material
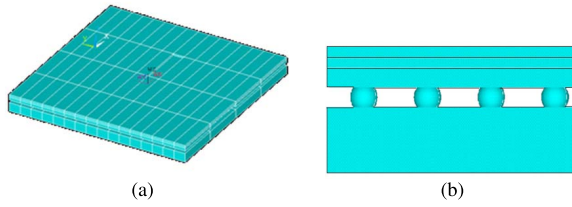
Fig. 12. (a) FEA model. (b) Simplified solder joint model.

TABLE VII
MATERIAL PROPERTIES FOR FEA

Structure or Material	Young's modulus (GPa)	CTE (10^{-6}/°C)	Poisson Ratio
Encapsulated layer	16.7	1.5	0.28
Chip(Si)	150.9	2.5	0.42
Substrate	29	15	0.3
PCB(FR4)	22	19	0.29
96.5Sn3.5Ag	30	26	0.45
96.5Sn3Ag0.5Cu	35	30	0.55
95.5SnAg0.5Cu	32	28	0.5
97.5Sn3.8AgCu	40	38	0.6

and dimension of solder joint, which is the problem found in Section III; then, the final form of the nonlinear accumulation rule could be obtained.

A. Modeling and Material Properties

A typical BGA package was modeled with the finite-element method using ANSYS; the results are shown in Fig. 12. The model contained solder joint, chip, substrate, encapsulated layer, and PCB layer. In ANSYS, element-type Visco107 was used to describe the solder joint material.

To evaluate the impact of solder joint material and dimension on the accumulation rule, four types of solder joint materials were selected. These were 96.5Sn3.5Ag, 96.5Sn3Ag0.5Cu, 95.5SnAg0.5Cu, and 97.5Sn3.8AgCu, and the diameters of the solder joint were selected as 0.5, 0.25, 0.4, and 0.6 mm. The "Anand" constitutive function was used to describe the creep property of the solder joint material [31]. Furthermore, the material properties of solder joint were identical to [31]. Table VII shows further material properties used for FEA modeling.

Boundary conditions were applied to the model, which included symmetric boundary condition, middle layer displacement coupled boundary condition, and fixed condition on the origin of coordinate. These boundary conditions simulated real usage conditions of solder joints [31]. Temperature profiles (shown in Figs. 3 and 4) were applied to the FEA model.

B. Simulation Results

The solder joint strain could be calculated via FEA. With the relationship of mechanical strain and resistance strain of solder joint under thermal damage, the daisy chain resistance could be obtained [32]. Fig. 13 shows the resistance of T1 obtained via experimental group 1 and FEA.
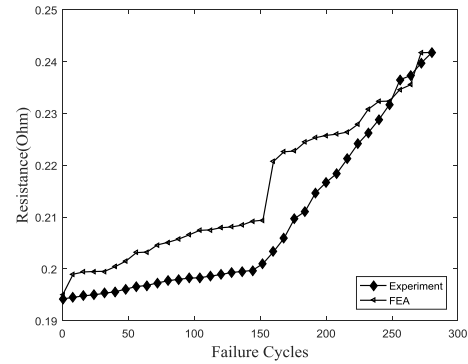

Fig. 13. Resistance of the T1 daisy chain via experimental group 1 and FEA.

TABLE VIII
PARAMETERS A AND B OF DIFFERENT SOLDER JOINT
DIAMETERS AND MATERIALS

Material	Diameter (mm)	Young's modulus E (GPa)	Fatigue strength factor σ_f (GPa)	a	b
96.5Sn 3.5Ag	0.5	30	1.97	2.759	-0.867
	0.4	30	1.97	2.758	-0.856
	0.25	30	1.97	2.846	-0.853
	0.6	30	1.97	2.824	-0.848
96.5Sn 3Ag 0.5Cu	0.5	35	2.25	2.812	-1.163
	0.4	35	2.25	2.832	-1.209
	0.25	35	2.25	2.782	-1.171
	0.6	35	2.25	2.797	-1.221
95.5Sn Ag 0.5Cu	0.5	32	2.01	2.824	-0.925
	0.4	32	2.01	2.767	-0.936
	0.25	32	2.01	2.800	-0.944
	0.6	32	2.01	2.785	-0.935
97.5Sn 3.8Ag Cu	0.5	40	2.55	2.831	-2.072
	0.4	40	2.55	2.835	-2.108
	0.25	40	2.55	2.839	-2.097
	0.6	40	2.55	2.759	-2.143

Fig. 13 shows that the simulation result was not as smooth as the experimental result, which was due to the mutation at the inflection point caused by computational assumptions. However, the error was controlled within 5%, which was considered to be reasonable within 20%.

C. Accumulation Rule Considering Material and Dimension

Using these simulation results, the parameters a and b in (7) for four material types and four diameters of solder joints could be calculated, and the results are shown in Table VIII. The material of the solder joint was expressed with Young's modulus and fatigue strength factor, which are the most critical parameters of the material for fatigue failure. Fig. 14 shows the relationship between parameters a and b depending on diameter and material of the solder joint.

Fig. 14(a) shows that the material and dimension of solder joints have no effect on parameter a. After testing, parameter a corresponds to a normal distribution, with a mean of 2.803 and a standard deviation of 0.03124

$$a \sim N(2.803, 0.03124^2).$$

Fig. 14(b) shows that parameter b changed with changing material; however, no significant relationship was detected
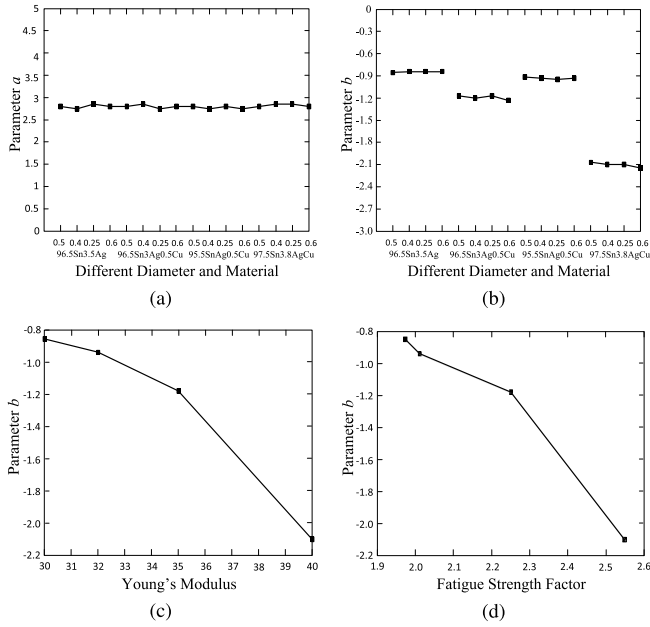
Fig. 14. Relationship of parameters a and b with diameter and material of solder joints. (a) Relationship of a with solder joint. (b) Relationship of b with solder joint diameter and material diameter and material. (c) Relationship of b with E. (d) Relationship of of b with σ_f.

TABLE IX
FAILURE CYCLES FROM EXPERIMENT AND SIMULATION

Group	Experiment cycles	Final form rule cycles	Error ratios	Rule with experiment results cycles	Error ratios
1	282	295	4.6%	296	5.0%
2	184	198	7.6%	194	5.4%
3	232	234	0.8%	236	1.7%
4	338	364	7.7%	357	5.6%

TABLE X
ACCELERATION TEST DATA

Solder joint of Component	Accelerated test of standard profile 1 (cycles)	Accelerated test of standard profile 2 (cycles)	Accelerated test of combined profile (cycles)	a	b
D1	7390	9252	6240		
D2	7434	9374	6345		
D3	7597	9575	6578	2.803	-3.9072
D4	7639	9739	6879		
D5	7849	10049	7020		

TABLE XI
COMPARISON OF SOLDER JOINT LIFE PREDICTION RESULTS

Solder joint of Component	Accelerated test results (cycles)	Estimated by Miner's rule (cycles)	Error ratios	Estimated by the proposed nonlinear rule (cycles)	Error ratios
D1	6240	4108	-34.2%	6526	4.6%
D2	6345	4146	-34.7%	6584	3.8%
D3	6578	4236	-35.6%	6727	2.3%
D4	6879	4281	-37.8%	6795	-1.2%
D5	7020	4406	-37.2%	6993	-0.4%

between parameter b and the dimension of solder joints for the same material. Fig. 14(c) and (d) shows that with the increase of Young's modulus E and fatigue strength factor σ_f, parameter b decreased. When these two variables were considered together, we found that they obey the ternary linear relationship after data fitting. Their relationship was assumed to be

$$b = c_1 + c_2 E + c_3 \sigma_f. \tag{21}$$

With the simulation results of FEA, the parameters in (21) were

$$c_1 = 3.28, \quad c_2 = -0.034, \quad c_3 = -1.56.$$

Furthermore, (7) can be expressed as

$$\begin{aligned}
N &= \frac{N_1}{(1 + (N_2/N_1)^b)^{\frac{1}{a}}} \\
a &\sim N(2.803, 0.03124^2) \\
b &= c_1 + c_2 E + c_3 \sigma_f \\
c_1 &= 3.28, \quad c_2 = -0.034, \quad c_3 = -1.56.
\end{aligned} \tag{22}$$

Young's modulus E and fatigue strength factor σ_f can be directly found within a material handbook. Equation (22) shows the final form of the nonlinear accumulation rule, which was applied to predict the thermal fatigue life of solder joints under an irregular temperature profile.

D. Discussion

Table IX shows the failure cycles obtained via experiment and that were calculated by (22) and the proposed nonlinear rule with the experimental results of Section III. The error

ratios between experiment and calculated values are also listed in Table IX.

Table IX shows that the error ratios between the failure cycles (calculated by the final form of the nonlinear accumulation rule and experiment values) could be controlled within 8%. Furthermore, some of the cycles from simulation were even closer to the actual values than those calculated via experiment results.

To verify the validity of the conclusion, we selected an avionics device for an accelerated test, and the data are shown in Table X. Here, the material of the solder joint was 98.5Sn3.8Ag0.5Cu, which utilized a Young's modulus E of 43 GPa and a fatigue strength factor σ_f of 3.67 GPa. Both standard profiles ranged from 50 °C to 70 °C and from 70 °C to 30 °C, respectively. Then, the solder joint lives for some PBGA components were achieved, as shown in Table XI.

The results show that with Miner's rule, the life of the solder joint tends to be underestimated, and the error ratio even reached a decrease of 37.8%, which is far beyond the

scope of the error. The root causes of these large errors can be divided into the following three points.

1) The relationship between damage D and failure cycle N is not linear, but exponential as shown in (3).
2) The relationship between stress σ and failure cycle N was exponential too as shown in (6).
3) The damage nucleus number m remained the same when stress σ_1 changed to σ_2, which is shown in Fig. 1(c). The damage curve 2 was changed to curve 3 in the combined temperature profile.

However, the prediction of solder joint life with the proposed nonlinear accumulation rule was much closer to the test results, and the error could be controlled within 5%, confirming the validity of the nonlinear accumulation rule proposed in this paper.

V. Conclusion

This paper presents a nonlinear accumulation rule for the prediction of solder joint life under combined profile, which can be segmented into two standard temperature cycles. Based on the fatigue crack propagation theory and the solder joint crack growth model, the equivalent damage under both segmented standard temperature cycles can be calculated with the damage curve and summarized to achieve the accumulation rule.

To determine the constants of the nonlinear accumulation rule, experiments were conducted under two regular profiles and their combined irregular profile. Surface-mounted BGA with diameters of 0.25 and 0.5 mm and two materials of 96.5Sn3.5Ag and 96.5Sn3Ag0.5Cu solder were selected. The four groups of temperature cycle experiments, each of which had three profiles, were conducted in a temperature chamber. Experiments stopped when the failure criterion achieved a 20% increase of nominal resistance of the daisy chain.

All results of four groups of experiments show that the sum of the damage for solder joint under both standard profiles were different from their combined complex cycles, indicating that the linear rule of accumulation is not applicable for this situation. In combination with the experimental data, the accumulation rules for the thermal fatigue damage of solder joints with a certain material and diameter were achieved and seemed to have a close relationship with material and diameter of the solder joint.

To study the relationship of the coefficients of the proposed nonlinear accumulation rule with the structure and material of the solder joint, the finite-element method was used to simulate more cases. The results show that parameters a and b have no relationship with solder joint dimensions. The solder joint material will not affect parameter a, but parameter b will decrease with increasing Young's modulus and fatigue strength factor. Consequently, a more general accumulation rule has been achieved. The comparison between accelerated test results and values calculated with the proposed nonlinear rule confirmed its validity.

This nonlinear accumulation rule solved problems existing in the previous studies and filled a vital gap. In particular, this rule can be extended to conditions of more standard cycles with varying amplitude, happening in sequence. This is a planned future study by our group. Furthermore, this rule is a bit overestimated the life cycles. A further study may focus on additional FEA simulations and study other factors that may affect nonlinear accumulation rules, such as different mounted styles and different packaging materials of the chip.

References

[1] L. Xing, "Reliability evaluation of phased-mission systems with imperfect fault coverage and common-cause failures," *IEEE Trans. Rel.*, vol. 56, no. 1, pp. 58–68, Mar. 2007.

[2] Y. Chen, L. Yang, C. Ye, and R. Kang, "Failure mechanism dependence and reliability evaluation of non-repairable system," *Rel. Eng. Syst. Safety*, vol. 138, pp. 273–283, Jun. 2015.

[3] Y. Y. Li, Y. Chen, Z. H. Yuan, N. Tang, and R. Kang, "Reliability analysis of multi-state systems subject to failure mechanism dependence based on a combination method," *Rel. Eng. Syst. Safety*, vol. 166, pp. 109–123, Oct. 2017.

[4] P. Borgesen *et al.*, "Solder joint reliability under realistic service conditions," *Microelectron. Rel.*, vol. 53, nos. 9–11, pp. 1587–1591, 2013.

[5] D. B. Barker, J. Vodzak, A. Dasgupta, and M. Pecht, "Combined vibrational and thermal solder joint fatigue—A generalized strain versus life approach," *ASME J. Electron. Packag.*, vol. 112, no. 2, pp. 129–134, 1990.

[6] P. Yang, D. Liu, Y. Zhao, Y. Tang, and H. Wang, "Approach on the life-prediction of solder joint for electronic packaging under combined loading," *IEEE Trans. Rel.*, vol. 62, no. 4, pp. 870–875, Dec. 2013.

[7] J. H. L. Pang, F. X. Che, and T. H. Low, "Vibration fatigue analysis for FCOB solder joints," in *Proc. IEEE Electron. Compon. Technol. Conf.*, vol. 1, Jun. 2004, pp. 1055–1061.

[8] A. Perkins and S. K. Sitaraman, "Vibration-induced solder joint failure of a ceramic column grid array (CCGA) package," in *Proc. IEEE Electron. Compon. Technol. Conf.*, vol. 2, Jun. 2004, pp. 1271–1278.

[9] M. Pei, X. Fan, and P. K. Bhatti, "Field condition reliability assessment for SnPb and SnAgCu solder joints in power cycling including mini cycles," in *Proc. IEEE Electron. Compon. Technol. Conf.*, vol. 7, May/Jun. 2006, pp. 899–905.

[10] F. Chai, M. Osterman, and M. Pecht, "Strain-range-based solder life predictions under temperature cycling with varying amplitude and mean," *IEEE Trans. Device Mater. Rel.*, vol. 14, no. 1, pp. 351–357, Mar. 2014.

[11] C. Basaran and R. Chandaroy, "Thermomechanical analysis of solder joints under thermal and vibrational loading," *J. Electron. Packag.*, vol. 124, no. 1, pp. 60–66, 2002.

[12] A. Perkins and S. K. Sitaraman, "A study into the sequencing of thermal cycling and vibration tests," in *Proc. IEEE Electron. Compon. Technol. Conf.*, May 2008, pp. 584–592.

[13] L. Yang, L. Yin, B. Arafei, B. Roggeman, and P. Borgesen, "On the assessment of the life of SnAgCu solder joints in cycling with varying amplitudes," *IEEE Trans. Compon., Packag., Manuf. Technol.*, vol. 3, no. 3, pp. 430–440, Mar. 2013.

[14] P. Borgesen, L. Yang, A. Qasaimeh, and B. Arfaei, "Damage accumulation in Pb-free solder joints for complex loading histories," in *Proc. Pan Pacific Microelectron. Symp.*, 2011, pp. 18–20.

[15] C. K. Lin and H. Y. Teng, "Creep properties of Sn-3.5Ag-0.5Cu lead-free solder under step-loading," *J. Mater. Sci. Mater. Electron.*, vol. 17, no. 8, pp. 577–586, 2006.

[16] O. Jin, H. Lee, and S. Mall, "Investigation into cumulative damage rules to predict fretting fatigue life of Ti-6Al-4V under two-level block loading condition," *J. Eng. Mater. Technol., Trans. ASME*, vol. 125, no. 3, pp. 315–323, 2003.

[17] H. Y. Qi, M. Osterman, and M. Pecht, "A rapid life-prediction approach for PBGA solder joints under combined thermal cycling and vibration loading conditions," *IEEE Trans. Compon. Packag. Technol.*, vol. 32, no. 2, pp. 283–292, Jun. 2009.

[18] S. S. Manson and G. R. Halford, "Practical implementation of the double linear damage rule and damage curve approach for treating cumulative fatigue damage," *Int. J. Fracture*, vol. 17, no. 2, pp. 169–192, 1981.

[19] A. Singh, "Development and validation of an S-N based two phase bending fatigue life prediction model," *J. Mech. Des.*, vol. 125, no. 3, pp. 540–544, 2003.

[20] S. M. Marco and W. L. Starkey, "A concept of fatigue damage," *Trans. ASME*, vol. 76, no. 4, pp. 627–632, 1954.

[21] J. B. Kommers, "Effect of overstressing and understressing in fatigue," *Proc. Amer. Soc. for Test. Mater.*, vol. 38, pp. 249–268, Jan. 1938.

[22] H. Huang, "Calculation of fuzzy reliability in the case of random stress and fuzzy fatigue strength," *Chin. J. Mech. Eng.*, vol. 13, no. 3, pp. 197–200, 2000.

[23] G. R. Halford, "The energy required for fatigue (Plastic strain hystersis energy required for fatigue in ferrous and nonferrous metals)," *J. Mater.*, vol. 1, no. 1, pp. 3–18, 1966.

[24] X. Niu, G. Li, and H. Lee, "Hardening law and fatigue damage of a cyclic hardening metal," *Eng. Fracture Mech.*, vol. 26, no. 2, pp. 163–170, 1987.

[25] W. Engelmaier, "Fatigue life of leadless chip carrier solder joints during power cycling," *IEEE Trans. Compon., Hybrids, Manuf. Technol.*, vol. CHMT-6, no. 3, pp. 232–237, Sep. 1983.

[26] S. S. Manson, J. C. Freche, and C. R. Ensign, "Application of a double linear damage rule to cumulative fatigue," in *Proc. Fatigue Crack Propag. ASTM Int.*, 1967, pp. 384–412.

[27] R. G. Forman and V. Shivakumar, "Growth behavior of surface cracks in the circumferential plane of solid and hollow cylinders," in *Proc. 17th Fracture Mech.*, 1986, pp. 345–349.

[28] *Standard Test Method for Fatigue Crack Growth Rates of Metallic Materials*, document GB/T6398-2000, National standards of People's Republic of China, 2000.

[29] J. Zhang, "Research on the size effect of creep damage of lead-free solder joint under shear tension," Ph.D. dissertation, School Phys. Electron., Central South Univ., Changsha, China, 2012.

[30] FIDES Group. (September 2010). *FIDES Guide 2009, Edition A: Reliability Methodology for Electronic Systems*. [Online]. Available: http://www.fides-reliability.org/files/UTE_Guide_FIDES_2009_Ed_A_EN.pdf

[31] C. Ying, H. Zebing, and K. Rui, "Lifetime prediction and impact factors analysis of ball grid array solder joint based on FEA," in *Proc. IEEE Int. Conf. Electron. Packag. Technol. High Density Packag.*, Aug. 2010, pp. 1142–1146.

[32] L. Jiang, "Theory and application of lead-free solder joint thermal damage electrical measurement," Ph.D. dissertation, School Energy Sci. Eng., Central South Univ., Changsha, China, 2009.

Ying Chen, photograph and biography not available at the time of publication.

Weiyang Men, photograph and biography not available at the time of publication.

Zenghui Yuan, photograph and biography not available at the time of publication.

Rui Kang, photograph and biography not available at the time of publication.

Ali Mosleh, photograph and biography not available at the time of publication.